

# 1 Thermally activated processes in an organic long-persistent luminescent system

2 Kazuya Jinnai,<sup>a,b</sup> Naohiro Nishimura,<sup>a,b</sup> Chihaya Adachi,<sup>\*a,b,c</sup> and Ryota Kabe<sup>\*b,d</sup>

3 <sup>a</sup> Center for Organic Photonics and Electronics Research (OPERA), Kyushu University, 744  
4 Motoooka, Nishi-ku, Fukuoka 819-0395, Japan

5 <sup>b</sup> JST, ERATO Adachi Molecular Exciton Engineering Project, 744 Motoooka, Nishi-ku,  
6 Fukuoka 819-0395, Japan

7 <sup>c</sup> International Institute for Carbon Neutral Energy Research (I2CNER), Kyushu University, 744  
8 Motoooka, Nishi-ku, Fukuoka 819-0395, Japan

9 <sup>d</sup> Organic Optoelectronics Unit, Okinawa Institute of Science and Technology Graduate  
10 University, 1919-1 Tancha, Onna-son, Kunigami-gun, Okinawa 904-0495, Japan

11  
12 E-mail: ryota.kabe@oist.jp; adachi@cstf.kyushu-u.ac.jp

## 13 Abstract

14  
15 Glow-in-the dark materials can store absorbed photon energy and emit light for long  
16 periods. While inorganic long-persistent luminescent (LPL) materials are crystalline and often  
17 require rare metals, organic LPL (OLPL) materials are flexible and require no rare metals. The  
18 emission process of OLPL systems consists of photo-induced charge separation, charge  
19 accumulation, and emission from charge recombination. Although emission processes of OLPL  
20 systems have been investigated, the charge separation and accumulation processes remain  
21 enigmatic. In this study, we investigated the charge carrier dynamics of a binary OLPL system  
22 comprising of electron donors and acceptors. We confirmed the presence of a thermal activation  
23 process, resembling thermally activated delayed fluorescence and thermoluminescence in the  
24 OLPL system.

## 25 1. Introduction

26  
27 Glow-in-the dark materials, which can store absorbed photon energy and emit light for long  
28 periods, are currently made entirely of inorganic materials.<sup>1,2</sup> Inorganic long-persistent  
29 luminescent (LPL) materials are used as light sources that do not require electrical power, as in  
30 emergency signs and watch dials. Inorganic LPL materials have good luminescent properties and  
31 durability, but require various fabrication processes like powdering and dispersing into polymeric  
32 media, because of their insoluble crystalline properties. High-performance LPL materials also  
33 require rare metal dopants.<sup>1,2</sup>

34 In contrast, organic LPL (OLPL) systems,<sup>3</sup> consisting of organic electron donors and  
35 acceptors, do not require rare metals and can form transparent and flexible films by solution

[ここに入力]

36 processes<sup>4,5</sup>. Unlike long-lived phosphorescence,<sup>6,7</sup> which is a radiative transition from a triplet  
37 excited state to a singlet ground state, OLPL systems accumulate energy in charge-separated states,  
38 similar to inorganic LPL systems.<sup>8,9</sup> While long-lived phosphorescence shows simple  
39 exponential emission decay, the emission from charge recombination is a higher-order reaction  
40 and frequently shows emission decay according to the power-law.<sup>10</sup> Thus, the LPL decay is  
41 empirically fitted by the following power-law equation.<sup>11</sup>

$$45 \quad I(t) = \frac{I_0}{(1 + At)^m} \quad (1)$$

42 Here,  $A$  ( $s^{-1}$ ) is the rate constant of the entire emission process and  $m$  is a parameter that depends  
43 on the materials ( $0.5 < m < 2$ ). However, each parameter depends on the number of accumulated  
44 carriers that are affected by the emission intensity and irradiation time.<sup>12</sup>

46 The emission process of OLPL systems consists of photo-induced charge separation, charge  
47 accumulation, and emission from charge recombination. The mixture of electron donors and  
48 acceptors forms the charge-transfer (CT) excited state between them, which is called an exciplex,  
49 after photoexcitation (**Figure 1**).<sup>13</sup> Then, some of the CT excited states become radical ion pairs  
50 of radical cationic donors and radical anionic acceptors.<sup>14</sup> After successive charge recombination  
51 of these radical ion pairs, CT excited states are regenerated and emit light from the CT excited  
52 state (Fig. 1(b)).

53 The charge recombination process generates both singlet and triplet CT excited states of  
54 exciplexes ( $^1\text{CT}$  and  $^3\text{CT}$ , respectively), but most of the emission is expected to occur from the  
55 radiative transition of  $^1\text{CT}$  since exciplexes exhibit thermally activated delayed fluorescence  
56 (TADF) through reverse intersystem crossing (RISC) due to the small energy gap ( $\Delta E_{\text{ST}}$ ) between  
57  $^1\text{CT}$  and  $^3\text{CT}$ .<sup>15,16</sup> Local triplet excited states of donors and acceptors ( $^3\text{LE}$ ) also influence the  
58 emission process. If the  $^1\text{CT}$  is the lowest excited state, LPL emission originates from the  $^1\text{CT}$ ,  
59 whereas if the  $^3\text{LE}$  is much lower than  $^1\text{CT}$ , LPL emission occurs from both  $^1\text{CT}$  and  $^3\text{LE}$ .<sup>8,9</sup>

60 Although emission processes of OLPL systems have been investigated, the charge separation

[ここに入力]

61 and accumulation processes remain to be unclarified yet. In this study, effects of excitation power  
62 intensity, excitation time, and sample temperature on photoluminescence (PL) and LPL intensities  
63 during photoexcitation were observed in order to understand the charge separation process. The  
64 initial PL process was also analyzed by time-resolved spectroscopy to understand the contribution  
65 of the charge separation process. The thermal activation process of OLPL was demonstrated by  
66 thermoluminescence (TL) measurements.

67

## 68 **2. Experimental Section**

69 *m*-MTDATA was obtained from Sigma-Aldrich (St. Louis, MA, USA). PPT was synthesized  
70 according to the literature.<sup>17</sup> All compounds were purified by sublimation and stored in a  
71 nitrogen-filled glovebox. The ~0.5-mm-thick mixed film was fabricated by the melt cast method.  
72 Mixtures of *m*-MTDATA (1 mol%) and PPT (99 mol%) were placed on a glass substrate with a  
73 1-cm<sup>2</sup> area recessed to a depth of 0.5 mm and heated to 250 °C for 30 s in a nitrogen-filled  
74 glovebox. After melting, the substrate was rapidly cooled to room temperature.

75 For time-resolved spectroscopy studies, a pulsed Nd:YAG laser (PL2250, EKSPLA) was used  
76 as an excitation source (excitation wavelength 355 nm, pulse width 20 ps). Sample emission was  
77 detected using a gated streak camera (C10910-04, Hamamatsu Photonics). The sample was placed  
78 in a cryostat (PS-HT-200, Nagase techno-engineering) connected to a turbo molecular pump  
79 (HiPace80, Pfeiffer vacuum) and temperature was controlled from 10 K to 500 K. The sample  
80 was excited by a 355-nm pulse laser (PL2210, Ekspla) at 10 Hz.

81 Temperature-dependence measurements and TL measurement were conducted in a cryostat  
82 (PS-HT-200, Nagase Techno-Engineering) connected to a turbo molecular pump (HiPace 80,  
83 Pfeiffer Vacuum). Emission spectra during (steady-state photoluminescence) and after (LPL)  
84 excitation were recorded using a multichannel spectrometer (QE-Pro, Ocean Photonics).  
85 Emission decay profiles of LPL were obtained using a Silicon photomultiplier (C13366-1350GA,  
86 Hamamatsu photonics) connected to a multimeter (34461A, Keysight).

[ここに入力]

87

88

### 89 3. Results and Discussion

#### 90 3.1 Photoluminescence with and without charge separation process

91 A mixed film of *m*-MTDATA as an electron donor, and PPT as an electron acceptor, was  
92 fabricated using a melt-cast process.<sup>18</sup> The sample was placed in a cryostat and was controlled  
93 from 10 K to 500 K under vacuum. The sample was photoexcited with a 355-nm pulsed laser  
94 (pulse width = 20 ps), and transient emission intensity and decay were recorded with a gated  
95 streak camera. The temperature dependence of emission decay profiles and time-resolved  
96 emission spectra are shown in **Figure 2**. Two exponential decays at nanosecond and microsecond  
97 timescales and a long emission tail of millisecond timescale were observed at room temperature  
98 (Fig. 1(a)). Emission spectra were slightly redshifted and then blueshifted over time (Fig. 1(d)),  
99 but most emission spectra are attributed to CT emission because they were broader than those of  
100 *m*-MTDATA and PPT (**Figure S1**). Within 10 ns after photoexcitation, the emission spectrum is  
101 slightly bluer than that of a steady-state PL spectrum due to *m*-MTDATA fluorescence, indicating  
102 insufficient CT formation.

103 The first exponential decay, at nanosecond timescale, corresponds to fluorescence of the  
104 exciplex, because the fluorescence lifetime ( $\tau_p$ ) of 350 ns is longer than that of *m*-MTDATA. The  
105  $\tau_p$  becomes longer at lower temperature due to suppression of the nonradiative decay. The second  
106 exponential decay ( $\tau_d = 21.5 \mu\text{s}$ ) corresponds to TADF, since the emission intensity increased and  
107  $\tau_d$  decreased by increasing the sample temperature (Fig. 2(f) and **Table S1**). Due to structural  
108 relaxation, the CT emission was slightly redshifted during the TADF process.<sup>19</sup>

109 The delayed emission after the TADF process corresponds to LPL emission, since the  
110 emission decay follows a power-law decay (Fig. 2(a)). Since LPL is not an exponential decay  
111 phenomenon, we cannot use the lifetime to discuss this long emission tail. The LPL emission  
112 spectra are identical to fluorescence spectra of exciplex, because the charge recombination

[ここに入力]

113 process generates both  $^1\text{CT}$  and  $^3\text{CT}$  states and the  $^3\text{CT}$  excitons are upconverted to  $^1\text{CT}$ . At 50 K,  
114 a power-law emission decay was observed from the microsecond timescale since the RISC  
115 process was suppressed (Fig. 2(b)). Although LPL by charge recombination is present in the  
116 whole-time scale, the LPL is difficult to observe at a short timescale, because the emission  
117 intensities of fluorescence and TADF are much stronger than that of LPL.

118

### 119 **3.2 Charge accumulation process**

120 Unlike long-lived phosphorescence, the charge separation process of the OLPL system  
121 requires greatly prolonged photoexcitation. LPL duration was observed by changing the  
122 photoexcitation time (**Figure 3**). LPL duration became longer and approached saturation as the  
123 excitation time increased (Fig. 3(b)). However, a slight increase was observed even with 1-hour  
124 photoexcitation, suggesting that more than 20 minutes of photoexcitation is required for sufficient  
125 charge accumulation. In the plot of excitation power intensity versus PL intensity (during  
126 photoexcitation) and integrated LPL intensity, the slope of the PL is 1, but that of LPL is close to  
127 0.5 (Fig. 3(c)). A slope of 1 indicates a single-photon process, since fluorescence without charge  
128 separation is dominant in the PL. In contrast, a slope of 0.5 indicates that LPL intensity is  
129 proportional to the square root of excitation intensity.<sup>20</sup>

130 The charge recombination process can be considered as either geminate ion  
131 recombination,<sup>21,22</sup> which means recombination between the original donor-acceptor pair, or as  
132 bulk recombination,<sup>23</sup> which means recombination between a different donor-acceptor pair. In  
133 the steady-state, generation rates of ion pairs,  $g$ , and the charge recombination rate,  $k_{\text{CR}}n^2$  are at  
134 equilibrium ( $k_{\text{CR}}$ ; charge recombination rate constant,  $n$ ; concentration of radical cation or radical  
135 anion). Because the generation rate of ion pairs is proportional to excitation intensity, the carrier  
136 concentration is proportional to the square root of the excitation intensity. A slope of 0.5 indicates  
137 that bulk recombination is the dominant process in this LPL emission. Previously, we reported  
138 that the LPL slope was close to 1 in the 3,3',5,5'-tetramethylbenzidine (TMB)/PPT system,<sup>4</sup> but

[ここに入力]

139 the TMB/PPT system exhibits strong room temperature phosphorescence since  ${}^3\text{LE}_D$  is lower than  
140  ${}^1\text{CT}$ . Because we used the intensity at 2 s after excitation in the previous report, the contribution  
141 of room temperature phosphorescence of TMB without charge separation (one photon process,  
142 slope = 1) was significant at that time range.

143 To understand the charge accumulation process, time-dependent PL intensities during  
144 photoexcitation were recorded (**Figures 4 and S2**). When the excitation power was constant, PL  
145 intensity gradually increased with time, due to the increased number of molecules excited by  
146 weak photoexcitation of  $1\ \mu\text{W}$  (Fig. 4(a, d)). When excitation power was  $10\ \mu\text{W}$ , the PL intensity  
147 increased for about 100 s and then became almost constant. With the excitation power of  $100\ \mu\text{W}$ ,  
148 the emission intensity reached its maximum in about 10 s and then decreased. Since charge  
149 accumulation is rapid at  $100\ \mu\text{W}$ , exciton quenching by accumulated excitons and polaron  
150 absorption by the accumulated charge is considered.<sup>24</sup>

151 When the excitation intensity is kept constant and the sample temperature is changed, the PL  
152 intensity reached its maximum in about 30 seconds and then became constant at 300 K (Fig. 4(b)).  
153 In contrast, the PL intensity quickly reached a maximum and then decreased at the low  
154 temperatures. Since charge diffusion is limited at low temperature, PL intensity saturates very  
155 quickly (**Figure 5**). At high temperatures such as 460 K, charge diffusion increases, but the effect  
156 of nonradiative deactivation also increases. Therefore, the PL intensity decreased over time. Since  
157 LPL is observed even at 10 K (Fig. 4(e)), charge recombination is thought to proceed via electron  
158 tunneling without thermal activation at low temperatures. The slope of LPL emission is nearly  $m$   
159 = 1 at room temperature, although it varies slightly with temperature and excitation intensity.  
160 When charge recombination proceeds by random walk after de-trapping, the slope is  $m = 1.5$ ,  
161 suggesting a contribution of electron tunneling, as well as thermal de-trapping.<sup>25</sup>

162 The donor/acceptor ratio is important for long-term charge accumulation, and the current  
163 optimum donor concentration is 1% for OLPL systems (Fig. 4 (f)). Although equal concentrations  
164 of donor and acceptor can form more exciplexes and are suitable for PL, charge carriers generated

[ここに入力]

165 by charge separation quickly recombine with neighboring donors when the donor concentration  
166 is high (Figs. 4(c), 5(c)).

167

### 168 **3.3 Thermoluminescence**

169 TL is often used to analyze inorganic LPL materials since the TL curve represents the trap  
170 depth of LPL systems.<sup>26</sup> The OLPL sample was kept at constant temperature (10, 100, 200, and  
171 300 K) in a cryostat and photoexcited with a 340-nm LED for 300 s. After photoexcitation, the  
172 initial LPL was observed. Then, the sample temperature was increased at 5 Kmin<sup>-1</sup> and TL  
173 intensity was obtained. Luminescence intensity was plotted against temperature to evaluate TL  
174 behavior.

175 When the TL measurement of the *m*-MTDATA/PPT film was started from 10 K, a clear TL  
176 curve peaked at around 120 K was observed. This TL curve indicates the presence of a thermal  
177 activation process in the OLPL system (**Figure 6**).<sup>27</sup> Note that the onset of the TL curve locates  
178 at around 50 K, which is much lower than that of inorganic LPL systems. When the TL  
179 measurement was started from 300 K, a very weak TL curve peaked at around 360 K was observed.  
180 These results indicate that the most of stored charge carriers of the *m*-MTDATA/PPT film can be  
181 detrapped and recombined until it reaches at room temperature. Thus, additional trap mechanisms  
182 like a ternary OLPL system<sup>4</sup> are required for efficient charge trapping.

183

### 184 **3.4 Oxygen quenching of OLPL**

185 Because the triplet excitons of TADF systems are often quenched by molecular oxygen,  
186 optical properties were also examined under oxygen gas (**Figure 7**). As a result, the LPL emission  
187 was quenched by oxygen. Since charges accumulate in the radical cation of *m*-MTDATA and the  
188 radical anion of PPT in the LPL system, the chemical reaction of radical species with oxygen  
189 should quench LPL emission. In contrast, interestingly TADF emission was not completely  
190 quenched by oxygen due to a very thick film.

[ここに入力]

191

## 192 4. Conclusions

193 We demonstrated the presence of thermal activation and TL in an *m*-MTDATA/PPT film. The  
194 TADF process represents not only the normal TADF process without charge separation, but also  
195 LPL from charge recombination. Therefore, triplet exciton management is important for highly  
196 efficient OLPL systems, similar to TADF OLEDs.

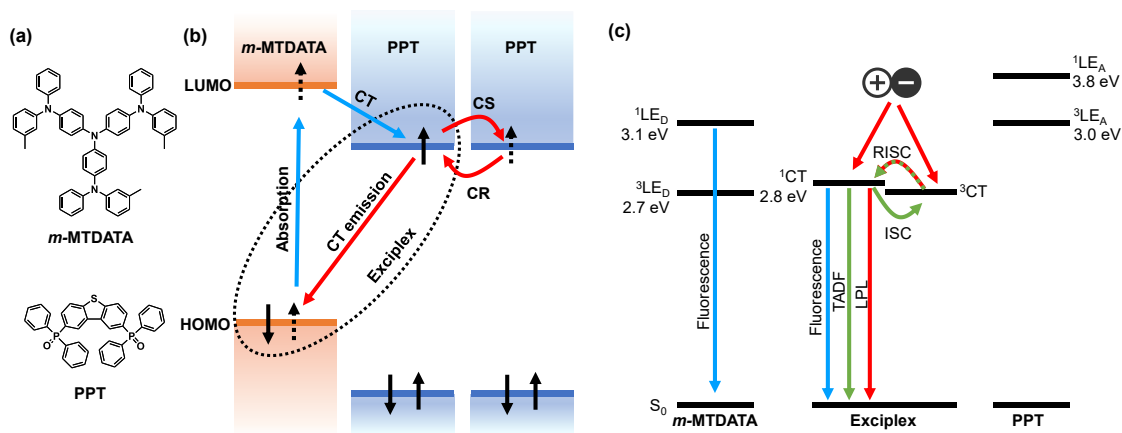
197

## 198 Acknowledgments

199 This work was supported by the Japan Science and Technology Agency (JST), ERATO,  
200 Adachi Molecular Exciton Engineering Project, under JST ERATO Grant Number JPMJER1305,  
201 Japan, JSPS core-to-core program, and JSPS KAKENHI Grant Numbers JP18H02049 and  
202 JP18H04522. We thank K. Kusuvara and N. Nakamura for their assistance with the preparation  
203 of PPT.

204

205

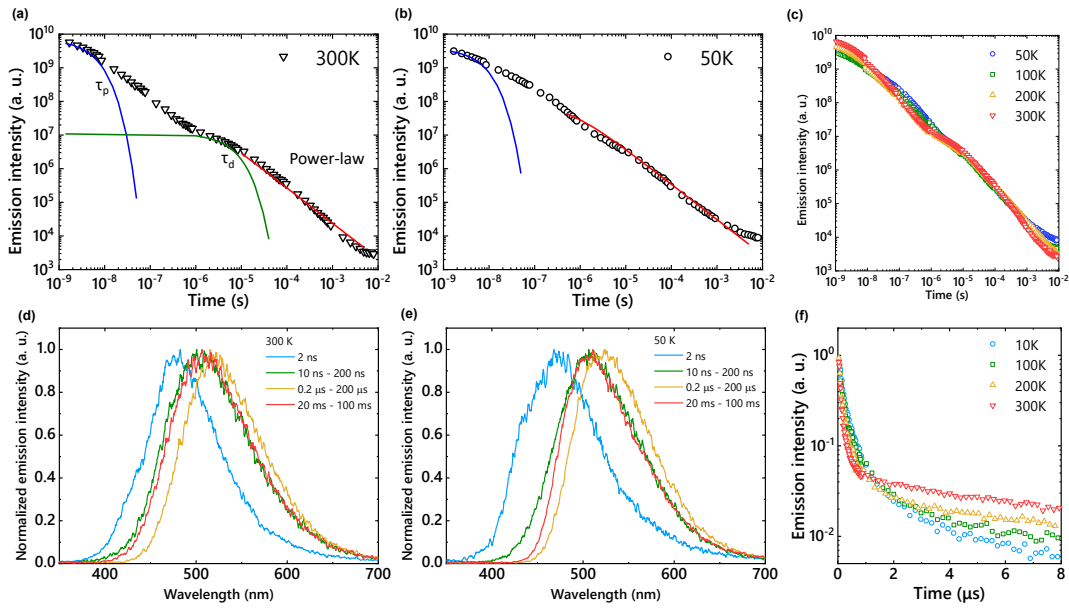


206

207 **Figure 1.** (a) Chemical structures of the electron donor, *m*-MTDATA, and the acceptor, PPT. (b)  
208 HOMO and LUMO energy diagrams and the emission mechanism of an OLPL system. (c) Singlet  
209 and triplet energy diagram of an *m*-MTDATA/PPT system. The OLPL system exhibits  
210 fluorescence, TADF, and LPL from the <sup>1</sup>CT state.

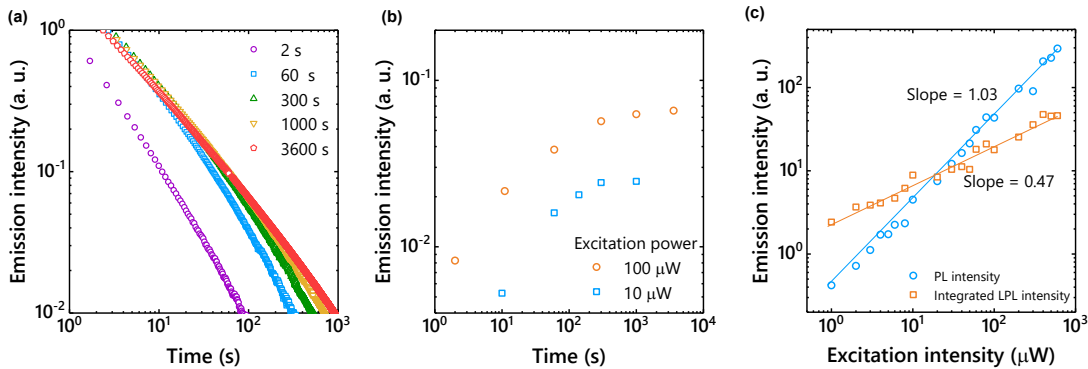
[ここに入力]





211

212 **Figure 2.** Emission decay profiles in a log-log plot of *m*-MTDATA/PPT film at 300 K (a), 50 K  
 213 (b), and various temperatures (c). Solid lines show fitting of  $\tau_p$ ,  $\tau_d$ , and power-law decay. Time-  
 214 dependent emission spectra at 300 K (d) and 50 K (e). Emission decay profiles in a semi-log plot  
 215 (f).

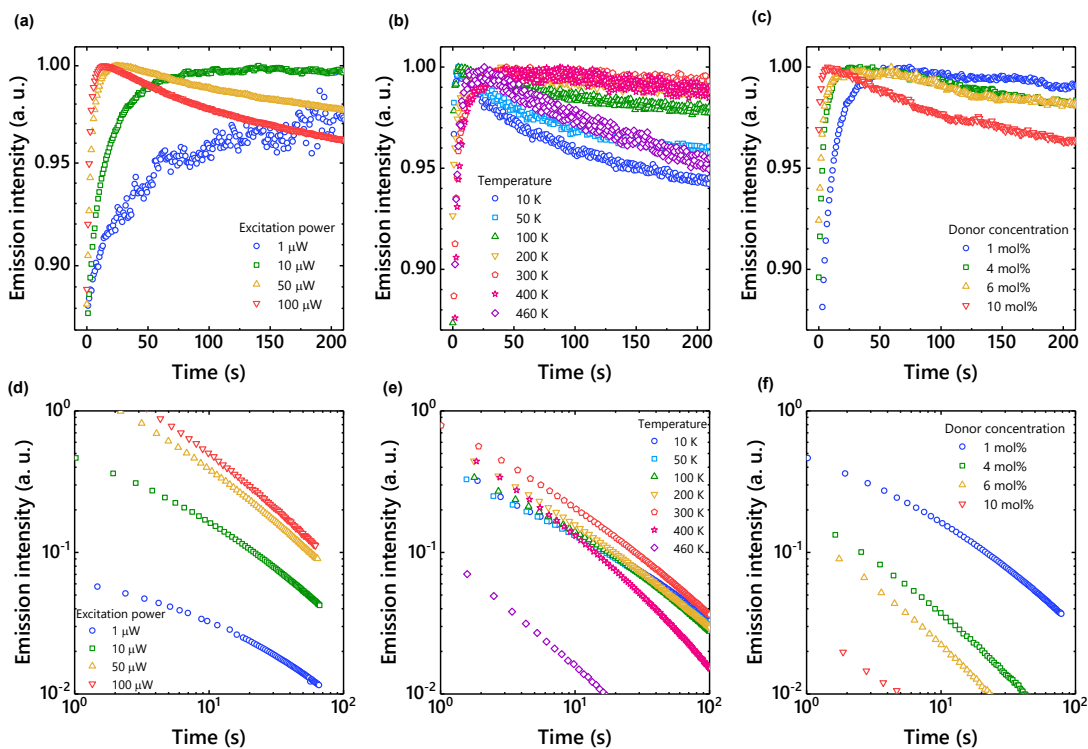


216

217 **Figure 3.** (a) Emission decay profiles showing the dependence of LPL on excitation time (1 molar  
 218 ratio of the donor; excitation power, 100  $\mu\text{W}$ ; temperature, 300 K). (b) Excitation-time  
 219 dependence of emission intensity 100 s after photoexcitation. (c) Excitation-power dependence  
 220 of emission intensity under photoexcitation (PL) and integrated LPL intensity. LPL intensity was  
 221 integrated from 100 s to 10000 s after photoexcitation. The solid lines show linear fitting.

222

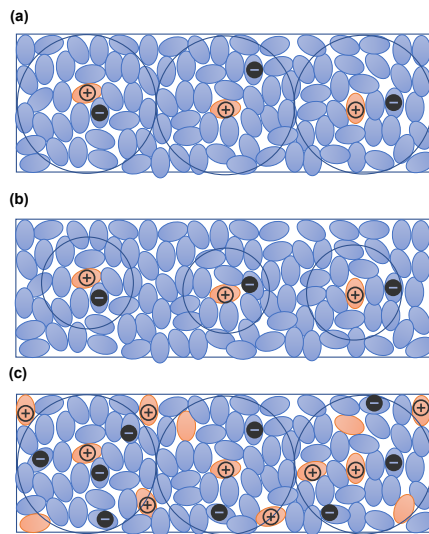
[ここに入力]



223

224 **Figure 4.** (a) Excitation power dependence of time-dependent emission intensity under  
 225 photoexcitation (1 molar ratio of the donor; temperature, 300 K). (b) Temperature dependence of  
 226 time-dependent emission intensity under photoexcitation (1 molar ratio of the donor; excitation  
 227 power, 10  $\mu$ W). (c) Donor concentration dependence of time-dependent emission intensity under  
 228 photoexcitation (excitation power, 10  $\mu$ W; temperature, 300 K). (d) Excitation power dependence  
 229 of time-dependent emission intensity after photoexcitation (1 molar ratio of the donor;  
 230 temperature, 300 K). (e) Temperature dependence of time-dependent emission intensity after  
 231 photoexcitation (1 molar ratio of the donor; excitation power, 10  $\mu$ W). (f) Donor concentration  
 232 dependence of time-dependent emission intensity after photoexcitation (excitation power, 10  $\mu$ W;  
 233 temperature, 300 K).  
 234

234

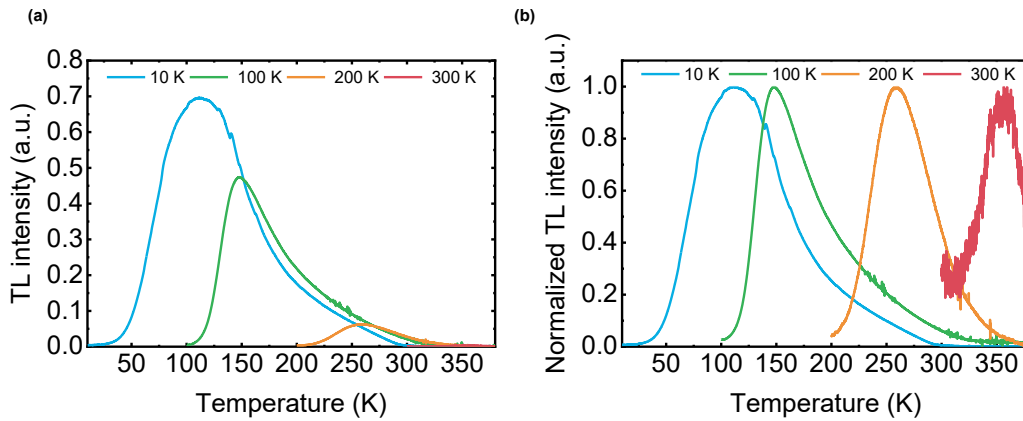


235

[ここに入力]

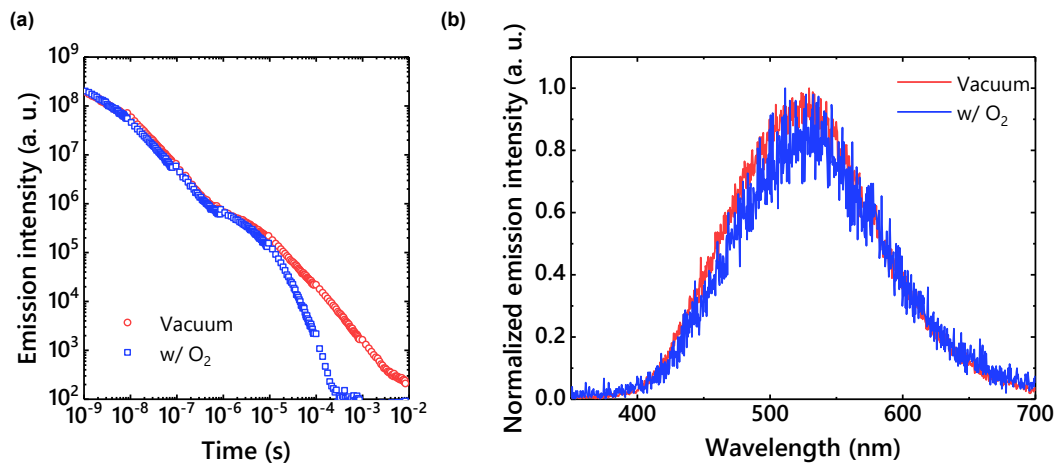
236 **Figure 5.** (a) Schematic diagram of a donor/acceptor mixed film. Charge separation occurs at the  
 237 interface between electron donors and acceptors. Due to the low donor concentration, holes are  
 238 localized to the donors and electrons diffuse to neighboring acceptor molecules. (b) Schematic  
 239 diagram of charge separation at low temperature. Electrons can diffuse shorter distances at low  
 240 temperature. (c) Schematic diagram of charge separation at a higher doping concentration.  
 241 Generated charges quickly recombine with neighboring donors.

242



243

244 **Figure 6.** (a) TL curves of an *m*-MTDATA/PPT film. Sample was photoexcited at the  
 245 starting temperature (10 K, 100 K, 200 K, and 300 K) for 300 s. After 1 h, sample  
 246 temperature was increased at 5 Kmin<sup>-1</sup>. (b) Normalized TL curves.



247

248 **Figure 7.** (a) An emission decay profile under vacuum and in air. The power-law decay  
 249 disappeared in air. (b) Delayed emission spectra under vacuum and in air.

250

251

[ここに入力]

1. J. Xu and S. Tanabe, *J. Lumin.*, 2019, **205**, 581.
2. S. Wu, Z. Pan, R. Chen and X. Liu, *Long Afterglow Phosphorescent Materials*, Springer International Publishing, Cham, 2017.
3. R. Kabe and C. Adachi, *Nature*, 2017, **550**, 384.
4. K. Jinnai, R. Kabe and C. Adachi, *Adv. Mater.*, 2018, **30**, 1800365.
5. Z. Lin, R. Kabe, N. Nishimura, K. Jinnai and C. Adachi, *Adv. Mater.*, 2018, **30**, 1803713.
6. S. Hirata, *Adv. Opt. Mater.*, 2017, **5**, 1700116.
7. Kenry, C. Chen and B. Liu, *Nat. Commun.*, 2019, **10**, 2111.
8. N. Nishimura, Z. Lin, K. Jinnai, R. Kabe and C. Adachi, *Adv. Funct. Mater.*, 2020, **30**, 2000795.
9. Z. Lin, R. Kabe, K. Wang and C. Adachi, *Nat. Commun.*, 2020, **11**, 191.
10. D. Hertel, H. Bässler, R. Guentner and U. Scherf, *J. Chem. Phys.*, 2001, **115**, 10007.
11. H. Ohkita, W. Sakai, A. Tsuchida and M. Yamamoto, *Bull. Chem. Soc. Jpn.*, 1997, **70**, 2665.
12. K. Gouda and Y. Hama, *Radiat. Phys. Chem.*, 1985, **26**, 285.
13. M. Sarma and K.-T. Wong, *ACS Appl. Mater. Interfaces*, 2018, **10**, 19279.
14. T. M. Clarke and J. R. Durrant, *Chem. Rev.*, 2010, **110**, 6736.
15. K. Goushi, K. Yoshida, K. Sato and C. Adachi, *Nat. Photonics*, 2012, **6**, 253.
16. H. Noda, X.-K. Chen, H. Nakanotani, T. Hosokai, M. Miyajima, N. Notsuka, Y. Kashima, J.-L. Brédas and C. Adachi, *Nat. Mater.*, 2019, **18**, 1084.
17. C. Fan, C. Duan, Y. Wei, D. Ding, H. Xu and W. Huang, *Chem. Mater.* 2015, **27**, 5131
18. K. Jinnai, N. Nishimura, R. Kabe and C. Adachi, *Chem. Lett.*, 2019, **48**, 270.
19. T. -C. Lin, M. Sarma, Y. -T. Chen, S. -H. Liu, K. -T. Lin, P. -Y. Chiang, W. -T. Chuang, Y. -C. Liu, H. -F. Hsu, W. -Y. Hung, W. -C. Tang, K. -T. Wong, and P. -T. Chou, *Nat. Commun.*, 2018, **9**, 3111.
20. K. Seki, K. Marumoto, and M. Tachiya, *Appl. Phys. Express*, 2013, **6**, 051603.
21. M. Wojcik, A. Nowak and K. Seki, *J. Chem. Phys.*, 2017, **146**, 054101.
22. K. Seki, K. Murayama and M. Tachiya, *Phys. Rev. B*, 2005, **71**, 235212.
23. J. S. Manser and P. V. Kamat, *Nat. Photonics*, 2014, **8**, 737.
24. D. Jia, *Opt. Mater.*, 2003, **22**, 65.
25. M. Tachiya and K. Seki, *Appl. Phys. Lett.*, 2009, **94**, 081104.
26. K. Van den Eeckhout, P. F. Smet and D. Poelman, *Materials*, 2010, **3**, 2536.
27. J. Ueda, K. Kuroishi, and S. Tanabe, *Appl. Phys. Lett.*, 2014, **104**, 101904